BIBF 1120: Triple Angiokinase Inhibitor with Sustained Receptor Blockade and Good Antitumor Efficacy

Frank Hilberg,[1] Gerald J. Roth,[2] Martin Krssak,[1] Susanna Kautschitsch,[1] Wolfgang Sommergruber,[1] Ulrike Tontsch-Grunt,[1] Pilar Garin-Chesa,[1] Gerd Bader,[1] Andreas Zoephel,[1] Jens Quant,[1] Armin Heckel,[2] and Wolfgang J. Rettig[1]

[1]Boehringer Ingelheim Austria GmbH, Vienna, Austria and [2]Boehringer Ingelheim Pharma GmbH & Co KG, Biberach, Germany

Abstract

Inhibition of tumor angiogenesis through blockade of the vascular endothelial growth factor (VEGF) signaling pathway is a novel treatment modality in oncology. Preclinical findings suggest that long-term clinical outcomes may improve with blockade of additional proangiogenic receptor tyrosine kinases: platelet-derived growth factor receptors (PDGFR) and fibroblast growth factor receptors (FGFR). BIBF 1120 is an indolinone derivative potently blocking VEGF receptor (VEGFR), PDGFR and FGFR kinase activity in enzymatic assays (IC_{50}, 20–100 nmol/L). BIBF 1120 inhibits mitogen-activated protein kinase and Akt signaling pathways in three cell types contributing to angiogenesis, endothelial cells, pericytes, and smooth muscle cells, resulting in inhibition of cell proliferation (EC_{50}, 10–80 nmol/L) and apoptosis. In all tumor models tested thus far, including human tumor xenografts growing in nude mice and a syngeneic rat tumor model, BIBF 1120 is highly active at well-tolerated doses (25–100 mg/kg daily p.o.), as measured by magnetic resonance imaging of tumor perfusion after 3 days, reducing vessel density and vessel integrity after 5 days, and inducing profound growth inhibition. A distinct pharmacodynamic feature of BIBF 1120 in cell culture is sustained pathway inhibition (up to 32 hours after 1-hour treatment), suggesting slow receptor off-kinetics. Although BIBF 1120 is rapidly metabolized *in vivo* by methylester cleavage, resulting in a short mean residence time, once daily oral dosing is fully efficacious in xenograft models. These distinctive pharmacokinetic and pharmacodynamic properties may help explain clinical observations with BIBF 1120, currently entering phase III clinical development. [Cancer Res 2008;68(12):4774–82]

Introduction

Targeted drugs interfering with the formation and maintenance of tumor blood vessels provide clinical benefit to cancer patients, including tumor regressions and prolonged survival, with acceptable tolerability (1, 2). Monoclonal antibodies to vascular endothelial growth factor (VEGF), notably bevacizumab (3), as well as small molecule inhibitors targeting the VEGF receptor (VEGFR) kinases, such as sunitinib and sorafenib (4), have been introduced into clinical practice and continue to be profiled in additional indications, alone or in combination with other treatment modalities. A next wave of antiangiogenic drug candidates is in clinical development, aiming to broaden the spectrum of cancer types or the proportion of patients that benefit from this new treatment modality (5–7).

From a mechanistic viewpoint, the concept of tumor angiogenesis has been refined since its early inception in the 1970s (8). The physiology of blood vessel formation and remodeling has been carefully dissected, showing that new capillaries form via a complex, tightly regulated process involving not only endothelial cells but also perivascular cells, such as pericytes and smooth muscle cells (9). The individual steps of angiogenesis, such as recruitment of endothelial precursor cells, endothelial cell proliferation, migration and survival, capillary tube formation, and pruning of capillary beds, were mapped and found to differ among normal and diseased tissues, with cancer vasculature being particularly aberrant in its composition and architecture (10).

Whereas the pivotal role of VEGF and VEGFR-2 in stimulating normal and disease-associated angiogenesis has been amply documented (11–17), it has become apparent that additional mechanisms may enhance or modulate this process, a consideration of potential importance in light of clinical experience with antiangiogenic drugs. Conceptually, the process of angiogenesis is of equal importance in all solid cancers, and yet there is wide variability in the extent to which current antiangiogenic drugs benefit individual patients. Relevant clinical factors include the organ type and stage of a given cancer, but most of the variability in tumor responsiveness is still unaccounted for. As clinical benefit seems to be transient in the majority of patients who initially respond to therapy (18, 19), several escape mechanisms have been considered. One particular line of evidence, based on preclinical animal models, suggests that targeting VEGF-VEGFR signaling and focusing on endothelial cells is beneficial at the start of treatment, but with continued drug treatment and under the pressure of VEGF signaling blockade resulting in increased hypoxia and malnutrition on the tumor cells, other signaling molecules and their cognate receptors provide alternate mechanisms to drive disease progression. Among the potential compensatory mechanisms, the platelet-derived growth factor (PDGF) and fibroblast growth factor (FGF) pathways—involving the PDGF receptors (PDGFR) important for signaling in perivascular smooth muscle cells and pericytes and FGF receptors (FGFR) that have been described as a potential escape mechanism with tumor cells switching from VEGF to FGF signaling to attract endothelial cells (20)—have been identified as promising targets for optimized drug candidates. In fact, the structural similarities between VEGFR, PDGFR, and FGFR tyrosine kinases provide a window for medicinal chemistry to design inhibitors that are active on all three kinase

Note: Supplementary data for this article are available at Cancer Research Online (http://cancerres.aacrjournals.org/).

Requests for reprints: Frank Hilberg, Boehringer Ingelheim Austria GmbH, Dr. Boehringer-Gasse 5-11, A-1121 Vienna, Austria. Phone: 43-1-80105-2351; Fax: 43-1-80105-2366; E-mail: frank.hilberg@vie.boehringer-ingelheim.com.

doi:10.1158/0008-5472.CAN-07-6307

families, yet retain the overall kinase selectivity profile indispensable for a safe and well-tolerated drug candidate (21).

In this report, we describe the preclinical profile of BIBF 1120, a combined VEGFR, FGFR, and PDGFR inhibitor currently entering phase III clinical studies in non–small cell lung carcinoma and other cancers. We present an analysis of BIBF 1120 in functional tests with three cell types known to contribute to tumor angiogenesis. For endothelial cells, pericytes, and smooth muscle cells, we provide *in vitro* biochemical analysis of signaling pathway modulation and assess effects on cell proliferation and survival. We further show that BIBF 1120, building on this pharmacologic profile, as well as distinct pharmacokinetic properties, is effective and well tolerated in multiple animal models of cancer.

Materials and Methods

Chemistry. The indolinone BIBF 1120 was derived from a chemical lead optimization program designed for receptor tyrosine kinase inhibitors (Patent Application WO01/27081, example 473).

Protein expression and X-ray crystallography. VEGFR-2 lacking the central kinase insert domain (T940-E989, E990V), as described in ref. 22, was cloned into a baculovirus vector. The construct contained, in addition, an NH_2 terminal glutathione *S*-transferase (GST) tag and a thrombin cleavage site. GST-VEGFR-2 was expressed in High-5 cells. Cell pellets were lysed by dounce homogenization in 20 mmol/L Tris-HCl, 20 mmol/L NaCl, 5 mmol/L DTT, supplemented with protease inhibitors (Complete, Roche; pH 8.0). The lysate was centrifuged for 45 min at 19,000 × *g*. GST-VEGFR-2 in the soluble fraction was bound to reduced glutathione Sepharose 4B resin (GE Healthcare), and the GST tag cleaved (on-column) with thrombin overnight. VEGFR-2 in the supernatant was phosphorylated *in vitro* by addition of $MgCl_2$ and ATP to 26 and 4 mmol/L, respectively. After concentration over Centricon-10 centrifugal concentrators (Millipore), VEGFR-2 was applied to a Superdex 75 HiLoad 16/60 size exclusion column (GE Healthcare) equilibrated with 20 mmol/L Tris-HCl, 20 mmol/L NaCl, and 5 mmol/L DTT (pH 8.0). VEGFR-2 containing fractions were pooled and concentrated to 8 mg/mL. Final material was aliquoted, frozen, and stored at −80°C. The protein was incubated with 1 mmol/L BIBF 1120 for 30 min at 4°C and was crystallized as previously described (22). The crystals appeared in 7 d and belonged to space group $P2_12_12_1$ with cell dimensions of a = 38.25, b = 94.44, and c = 96.22. The structure was solved by molecular replacement and refined at a resolution of 2.1 Å to a final R factor of 21.7% (R_{free} = 27.9%) using the CCP4 package (Collaborative Computational Project, Number 4. The CCP4 Suite: Programs for Protein Crystallography. Acta Cryst., 1994; D50: 760–3) and COOT (23), respectively. The atomic coordinates of the structure and the structure factors have been deposited in the protein databank with the accession code 3C7Q.

***In vitro* kinase activity assays.** The cytoplasmic tyrosine kinase domain of VEGFR-2 (residues 797–1355 according to sequence deposited in databank SWISS-PROT P35968) was cloned into pFastBac fused to GST and extracted as described in supplementary methods. Enzyme activity was assayed using standard conditions using a random polymer (Glu/Tyr 4:1; Sigma) and in the presence of 100 μmol/L ATP (for details, see supplementary methods). For all other kinase assays, the entire cytoplasmic domains of the receptors (from the end of the transmembrane to the COOH terminus) were cloned into pFastBac vector containing GST and assayed under standard conditions.

Human cancer cell lines and normal endothelial cells, pericytes, and smooth muscle cell cultures. Tumor cell lines FaDu (American Type Culture Collection, ATCC; HTB-43), Caki-1 (ATCC, HTB-46), HT-29 (ATCC, HTB-38), SKOV-3 (ATCC, HTB-77), H460 (ATCC, HTB-177), Calu-6 (ATCC, HTB-56), PAC-120 (24), and the rat glioma cell line GS-9L (25) were cultured in Iscove's modified Dulbecco's medium (IMDM; Life Technologies-Bethesda Research Laboratories #21980-032), supplemented with 10% FCS (Sigma), 50 μmol/L β-mercaptoethanol (for endothelial cell culture; Fluka #63689), and 100 units/mL penicillin/100 μg/mL streptomycin (P/S; BioWhittaker). Human umbilical vascular endothelial cell (HUVEC; Technoclone), human microvascular skin endothelial cells (HMSEC; Technoclone), human umbilical artery smooth muscle cells (HUASMC; Technoclone), and bovine retinal pericytes (BRP; for isolation, see supplementary methods) were grown in IMDM (Life Technologies-Bethesda Research Laboratories), 10% FCS (Sigma), 50 μmol/L β-mercaptoethanol (Fluka), and P/S (BioWhittaker). For HUVEC and HMSEC, 15 μg/mL endothelial cell growth supplement (ECGS; Collaborative Biomedical Products #4006) and 100 μg/mL heparin (Sigma H-3393) were added. These adherent cells were grown in gelatin-coated (Sigma G-1393) cell culture flasks at 37°C and 5% CO_2. For the assay, all cell types were starved overnight in medium without ECGS and heparin and with reduced FCS. On the day of the assay, the cells were trypsinized, and 2,500 cells per well were plated in 96-well plates (not gelatin-coated) in a volume of 200 μL IMDM (10% FCS, β-mercaptoethanol, P/S). Control cells did not receive additional growth factors, all the other cells were supplemented with 10 μg/mL heparin and either 5 ng/mL VEGF165 [human recombinant vascular endothelial growth factor (VEGF; R&D System #293VE050)] or 5 ng/mL basic FGF (bFGF; R&D Systems #234-FS) for the endothelial cells. SMCs and BRPs were stimulated with either bFGF or PDGF-BB (R&D Systems #220-BB), respectively.

Cell proliferation and apoptosis assays. [^{3}H]Thymidine incorporation assay for proliferation analysis and apoptosis assay was performed as previously described (26).

Inhibition of cell signaling cascades in drug-treated cells. HUVEC, HUASMC, and BRP were cultured as described above. Two hours before the addition of ligands, BIBF 1120 was added to the cultures. Cell lysates were generated according to standard protocols (Current protocols in molecular biology, edited by F.M. Ausubel, R. Brent, R.E. Kingston, D.D. Moore, J.G. Seidman, J.A. Smith & K. Struhl, 2004, John Wiley and Sons, Inc.). Western blotting was done using standard SDS-PAGE methods, loading 50 to 75 μg of protein per lane, with detection by enhanced chemiluminescence. Total and phosphorylated mitogen-activated protein kinase (MAPK) was analyzed using monoclonal antibodies M3807 and M8159 from Sigma, respectively. Total Akt was detected using the polyclonal antibody #9272 and phosphorylated Akt (Ser^{473}) was analyzed with the monoclonal antibody #4058 both from Cell Signaling. Cleaved caspase-3 was detected with the Cell Signaling monoclonal antibody #9665, and the polyclonal β-actin antibody was purchased from Cell Signaling (#4967). KDR (VEGFR-2) protein was detected using a specific antibody from Santa Cruz Biotechnology (#sc-315).

***In vivo* tumor models.** All experiments complied with the Declaration of Helsinki and European Policy Legislations (FELASA and GV-SOLAS) on the Care and Use of Laboratory Animals. Five-week-old to 6-wk-old athymic NMRI-nu/nu female mice (21–31 g) were purchased from Harlan (Germany). After acclimatization, mice were inoculated with 1 to 5 × 10^6 (in 100 μL) FaDu, Caki-1, SKOV-3, H460, HT-29, or PAC-120 cells s.c. into the right flank of the animal. F344 Fischer rats were purchased from Charles River and after acclimatization were injected with 5 × 10^6 (in 100 μL) GS-9L cells s.c. into the right flank of the animal. For pharmacokinetic analysis, blood was isolated at indicated time points from the retroorbital plexus of mice and plasma was analyzed using high performance liquid chromatography–mass spectrometry methodology.

Immunohistochemistry and image analysis. For the analysis of vessel density and vessel morphology in tumor xenografts, female athymic NMRI nude mice were grafted s.c. with the human FaDu cells, as described above. Mean tumor volume at the start of the experiment was ~100 mm^3. Tumors were excised after 5 d of administration of the compound and from the vehicle-treated mice. The tumors were embedded in OCT, snap frozen in liquid nitrogen, and stored at −80°C. Tumor sections were analyzed using the avidin-biotin complex (ABC) immunoperoxidase procedure as previously described (27). Briefly, 5-μm-thick sections were cut and mounted on poly-(Lysine)–coated slides. Sections were blocked with 10% serum from the host of the secondary antibody and incubated with the primary antibodies at the appropriate dilutions in PBS/2% bovine serum albumin for 1 h at room temperature. Biotinylated secondary antibodies were added at a 1:100 dilution, followed by Vectastin ABC solution 1:100 (Vector Labs). The binding of the antibodies was visualized with 3,3′-diaminobenzidine (DAB) solution (0.06% DAB in PBS, 0.003% H_2O_2). Slides were then dehydrated and

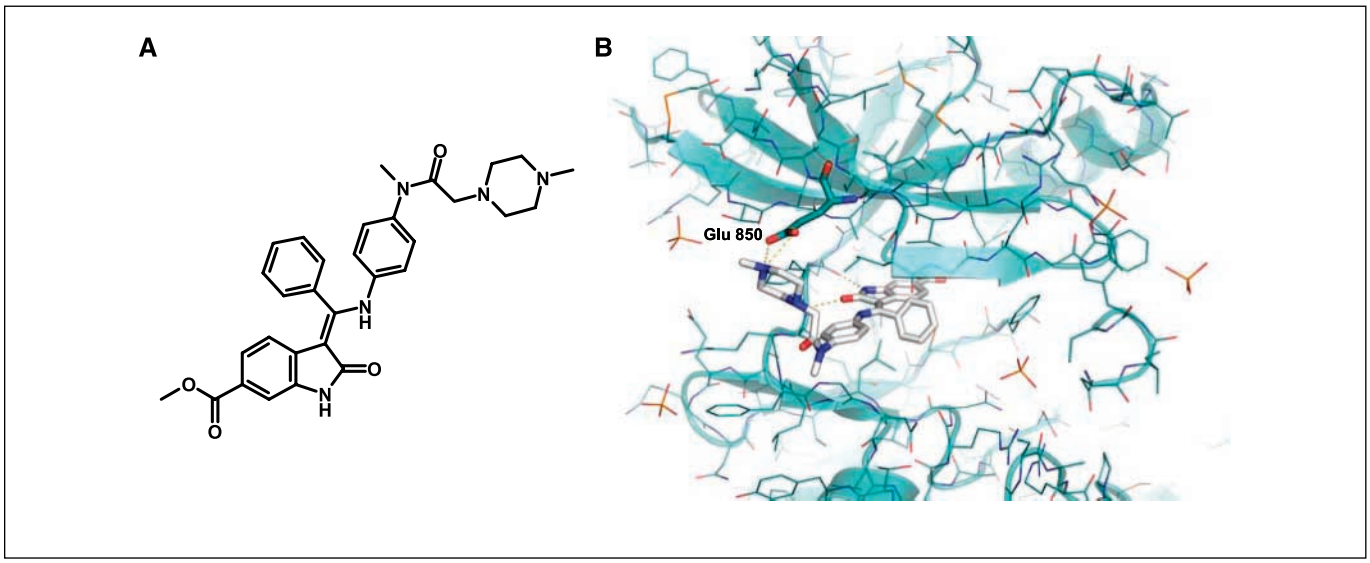

Figure 1. Chemical structure of BIBF 1120 (*A*) and X-ray structure of BIBF 1120 bound in the active site of the VEGFR-2 crystal (*B*). The hydrogen bonds of the indolinone scaffold to the hinge region and the ionic interactions between the *N*-methyl piperacyl-moiety of BIBF 1120 (*yellow dots*).

counterstained with Harris' hematoxylin. Colocalization studies for endothelial and pericyte markers were performed by double immunofluorescence methods. Detection was performed with Alexa 488 goat anti-rat and Alexa 594 goat anti-rabbit (Molecular Probes). Primary antibodies used included antimouse endothelial marker Meca 32 [rat monoclonal antibody (mAb), 1:1,000, BD PharMingen], anti-PDGFRβ (rabbit mAb 28E1, 1:100 dilution, Cell Signaling Technology, Inc.). For image analysis, the vessel density was determined on digital images obtained from 5-μm-thick stained sections of three control and three treated mice. From each animal, three representative pictures were obtained with a Zeiss Axiophot microscope at 10× magnification. Measurements were made using the Definiens Developer image analysis software (Definiens AG). The vessel area was determined by measuring the vascular structures that were reactive with the mouse specific antibody Meca 32 compared with the tumor parenchyma (tumor cells + tumor stroma, excluding normal tissues). The area of vessels covered by pericytes was determined on adjacent sections stained with the PDGFRβ antibody and calculated as described above. The significance between means was determined by the Student's *t* test ($P < 0.05$).

Dynamic contrast enhanced MRI. All experiments were performed in a PharmaScan 70/16 MR System (Bruker Biospin) using a standard 38-mm 1H volume resonator in transmit/receive mode. Tumor perfusion/permeability was determined by dynamic contrast enhanced (DCE) MRI (single slice two-dimensional T1 weighed FLASH, flip angle 30°, TE = 2.8 ms, TR = 13.5 ms, NA = 4, NR = 50) using Gd-DTPA (0.1 mmol/kg, Magnevist, Schering). Contrast agent was given into the tail vein as a short bolus (100 μL in ~2 s) immediately after the acquisition of the fifth image. Initial image analysis was done within Paravision Software package (Bruker BioSpin). Toft's model analysis (28) was used to assess the transfer constant (K^{TRANS}) as implemented in Jim 3.0 Image Analysis software package (Xinapse Systems Ltd.). Predefined arterial input function was extracted from a series of calibration measurements.

Results

Structure of BIBF 1120 bound to VEGFR-2 kinase. BIBF 1120, a substituted oxindole derivative, was synthesized in a chemical lead optimization program designed to identify ATP-competitive inhibitors of VEGFR-2 and other proangiogenic receptor tyrosine kinases. The expected binding mode was confirmed by cocrystallization with recombinant VEGFR-2 kinase and X-ray diffraction at a resolution of 2.1 Å (Fig. 1). BIBF 1120 binds to the ATP-binding site in the cleft between the NH_2 and COOH terminal lobes of the kinase domain. The indolinone scaffold forms two hydrogen bonds to the backbone nitrogen of Cys^{919} and the backbone carbonyl oxygen of Glu^{917} in the hinge region. The methyl piperacinyl group points into the solvent region. However, the 4-nitrogen atom of the *N*-methyl piperacinyl moiety forms a bidentate ionic interaction with the carboxylate oxygens of Glu^{850} with distances of 3.2 and 3.3Å, respectively. Sequence comparisons with the PDGFR kinase domain show a glutamate residue at an equivalent position (PDGFRα, Glu^{609}; PDGFRβ, Glu^{615}).

Kinase selectivity profile. Extensive biochemical testing revealed a distinctive, narrow range of kinases that are inhibited by BIBF 1120 at pharmacologically relevant concentrations. The targeted kinases include all three VEGFR subtypes (IC_{50}, 13–34 nmol/L), PDGFRα and PDGFRβ (IC_{50}, 59 and 65 nmol/L), and FGFR types 1, 2, and 3 (IC_{50}, 69, 37, and 108 nmol/L, respectively; Table 1). Comparable inhibition was seen for the corresponding human and rodent kinases. In addition, BIBF 1120 inhibits FLT3 (inhibition of acute myelogenous leukemia cell proliferation has been shown previously; ref. 29), as well as members of the Src-family (Src, Lyn, and Lck). By contrast, receptor tyrosine kinases, such as EGFR and HER2, InsR, IGF-IR, or the cell cycle kinases CDK1, CDK2, and CDK4 (Table 1) were not inhibited at concentrations below 1,000 nmol/L.

Signaling pathways, proliferation, and survival of endothelial cells. Treatment of VEGF-stimulated endothelial cells derived from umbilical veins (HUVEC) and skin microvessels (HSMEC) with BIBF 1120 resulted in inhibition of cell proliferation and apoptosis (EC_{50}, <10 nmol/L; Table 2) and was preceded by inhibition of MAPK and Akt phosphorylation (Fig. 2*A*). Inhibition of bFGF-stimulated HUVEC proliferation required higher drug concentrations (EC_{50}, 290 nmol/L), although activation of both MAPK and Akt was at least partially suppressed at concentrations down to 100 nmol/L. The apoptosis marker cleaved caspase-3 was up-regulated in a concentration-dependent manner in both VEGF-stimulated and bFGF-stimulated HUVEC, and the proportion of apoptotic HUVEC cells as measured by TUNEL stain increased

Table 1. *In vitro* kinase inhibition profile of BIBF 1120

Kinase	IC_{50} (nmol/L)*
VEGFR-1	34 ± 15
VEGFR-2	21 ± 13
VEGFR-2 (mouse)	13 ± 4
VEGFR-3	13 ± 10
FGFR-1	69 ± 70
FGFR-2	37 ± 2
FGFR-3	108 ± 41
FGFR-4	610 ± 117
PDGFRα	59 ± 71
PDGFRβ	65 ± 7
InsR	>4,000
IGF1R	>1,000
EGFR	>50,000
HER2	>50,000
CDK1	>10,000
CDK2	>10,000
CDK4	>10,000
Flt-3	26
Lck	16 ± 16
Lyn	195 ± 12
Src	156 ± 40
† Other kinases (n = 26)	>10,000

*Assays performed with ATP concentrations at the respective K_m. Human kinases were tested except when stated otherwise. Data represent mean ± SE of at least three determinations; IC_{50} values "greater than" indicate that half-maximum inhibition was not achieved at the highest concentration tested.

† Another 26 kinases were analyzed at 10 μmol/L with 100 μmol/L ATP: GSK3B, ROCKII, DYRK1A, PKCA, MAPK2ERK2, HGFR, MSK1, PDK1, CHK1, MAPKAPK2, SAPK2AP38, S6K1, SGK, CK1, CK2, PKA, SAPK2BP38B2, SAPK3P38G, JNK1A1, SAPK4P38D, PHK, PKBA, CSK, CDK2/CYCLINA, PRAK, PP2A (data not shown).

from 2% in control cells to 28% in the presence of 50 nmol/L BIBF 1120 (Supplementary Fig. S1*A*).

As a control experiment, we tested the effect of BIBF 1120 on the proliferation of human epithelial cancer cell lines FaDu, Calu-6, and HeLa, none of which expresses detectable VEGFR, FGFR, or PDGFR. None of these cell lines was inhibited at the highest concentration tested (3,500 nmol/L; Table 2).

Effects on pericytes and smooth muscle cells. Pericytes, important for vessel maturation and stabilization, are known to express PDGFRs (30). BIBF 1120 inhibited proliferation of PDGF-BB–stimulated BRPs with an EC_{50} of 79 nmol/L (Table 2), which is in general agreement with the biochemical kinase inhibition data. Signaling pathway analysis showed that activation of MAPK after stimulation with 5% serum plus PDGF-BB could be blocked by BIBF 1120 at concentrations down to 100 nmol/L. Stimulation of BRP with 5% serum plus bFGF blocked MAPK phosphorylation, but not concentration-dependently (Fig. 2*B*). Activation of Akt was clearly suppressed by BIBF 1120 after stimulation with PDGF-BB or bFGF down to a concentration of 100 nmol/L; interestingly, no increase in cleaved caspase-3 resulted from this pathway inhibition.

In cultures of human vascular smooth muscle cells (HUASMC), BIBF 1120 inhibited PDGF-BB stimulated proliferation with an EC_{50} of 69 nmol/L (Table 2), and MAPK activation was inhibited at concentrations down to 100 nmol/L. Cell lysates of HUASMC stimulated with bFGF showed inhibition of MAPK activation above concentrations of 300 nmol/L. Phosphorylation of Akt was completely blocked in bFGF or PDGF-BB stimulated HUASMC at BIBF 1120 concentrations as low as 100 nmol/L. Furthermore, the apoptosis marker cleaved caspase-3 was up-regulated in bFGF-stimulated HUASMC treated with BIBF 1120 (Fig. 2*C*).

Sustained VEGFR blockade. To determine the duration of VEGFR-2 inhibition by BIBF 1120, a pulse-chase experiment with VEGFR-2 transfected NIH3T3 cells (31) was performed. The cells were exposed for 1 hour to 50 nmol/L BIBF 1120, washed thoroughly with PBS, and incubated for 8, 24, or 32 hours in medium followed by stimulation with VEGF for 10 minutes. Western blot analysis of the cell lysates after immunoprecipitation revealed that inhibition of receptor phosphorylation was sustained for at least 32 hours after removal of BIBF 1120 (Supplementary Fig. S1*B*).

Rapid *in vivo* effects on tumor perfusion and permeability detected by DCE-MRI. Human FaDu (squamous cell carcinoma of the head and neck) xenografts growing in nude mice were analyzed by DCE-MRI using gadolinium contrast agent before and 72 hours after initiation of daily p.o. treatment with BIBF 1120 at 100 mg/kg. Tumor perfusion and vascular permeability was readily visible in the initial MRI scan and clearly reduced after 3 days of treatment (Fig. 3*A*); quantitation of the K^{TRANS} value showed a significant decrease in BIBF 1120–treated tumors compared with both baseline values and untreated controls (Fig. 3*A*).

BIBF 1120 affects tumor vessel density and pericytes. To confirm that BIBF 1120 affects the tumor vasculature, mice with established FaDu xenografts were treated for five consecutive days with either the vehicle control or BIBF 1120 at a dose of 100 mg/kg. After the last application, tumors were dissected and analyzed by immunohistochemistry using Meca 32 and PDGFRβ-specific

Table 2. Cellular effects of BIBF 1120 on growth factor–dependent proliferation, as determined by [^{3}H]thymidine incorporation in endothelial cells, smooth muscle cells, pericytes, and malignant epithelial cancer cells

Designation	Cell type	Growth factor	Growth inhibition EC_{50} (nmol/L)
HUVEC	Endothelial cell	VEGF	9 ± 13
		bFGF	290 ± 160
HSMEC	Endothelial cell	VEGF	7 ± 5
BRP	Pericyte	PDGF BB	79 ± 21
HUASMC	Vascular smooth muscle	PDGF BB	69 ± 29
FaDu	Epithelial cancer	In the presence of FCS	>4,500
Calu-6	Epithelial cancer	In the presence of FCS	>3,500
HeLa	Epithelial cancer	In the presence of FCS	>3,500

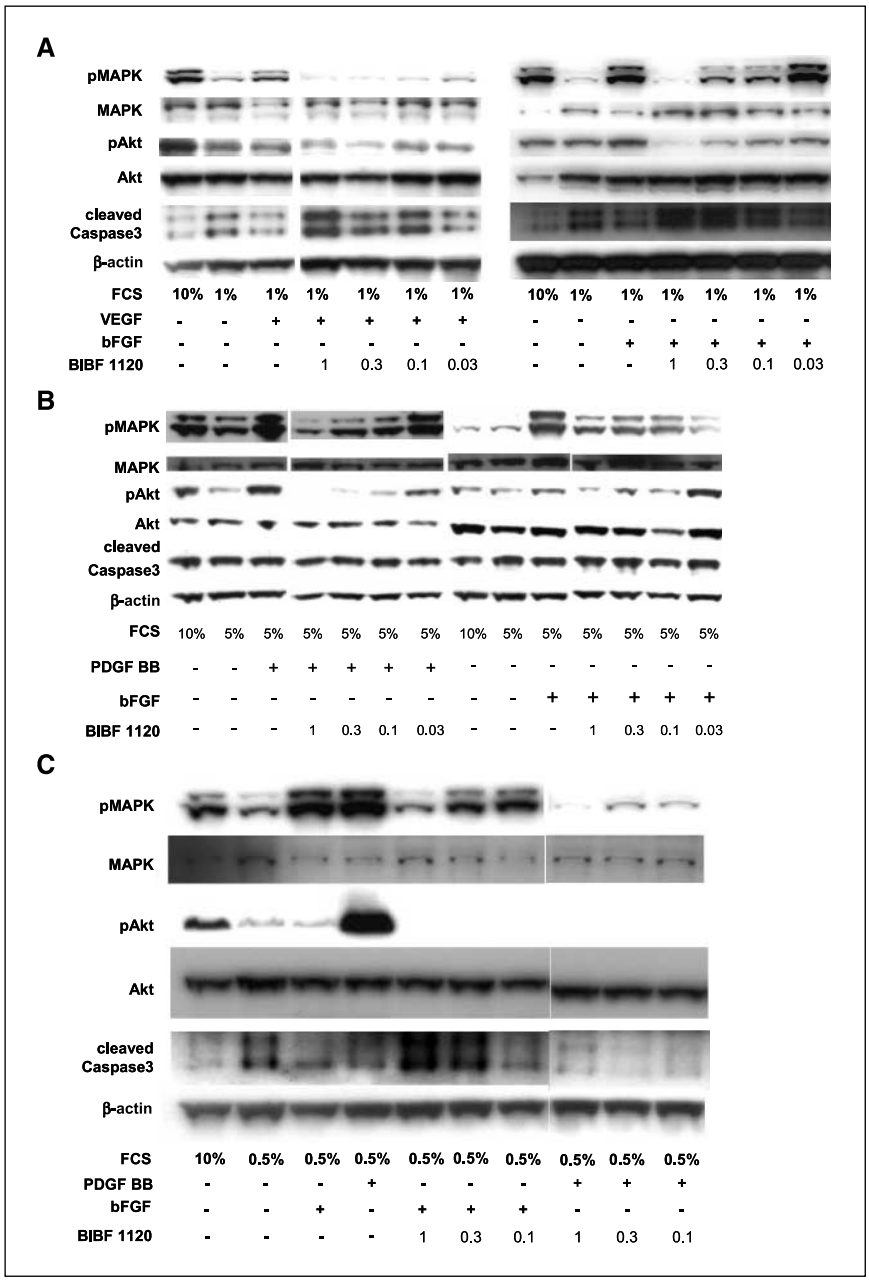

Figure 2. BIBF 1120 inhibits ligand-dependent phosphorylation of MAPK and Akt in human endothelial (HUVEC) and smooth muscle cells (HUASMC) and bovine retinal pericytes. Western blot analysis after exposure to BIBF 1120 of HUVEC stimulated with either VEGF or bFGF shows concentration-dependent reduction of phosphorylated MAPK and Akt levels and cleaved caspase-3 as an indicator for apoptosis (*A*); pericytes stimulated with PDGF-BB and bFGF show concentration-dependent reduction of phosphorylated MAPK and Akt levels (*B*). *C,* HUASMC stimulated with PDGF-BB and bFGF show concentration-dependent reduction of phosphorylated MAPK and Akt levels and cleaved caspase-3 as an indicator for apoptosis. BIBF 1120 concentrations are shown in μmol/L.

antibodies to stain endothelial cells and pericytes (Fig. 3*B*). In comparison to control tumors, vessel density in xenografts from mice treated with BIBF 1120 was reduced by 76% (Fig. 3*C*; $P < 0.001$). Quantification of PDGFRβ-positive mural cells showed a reduction of 64% after 5 days of treatment with BIBF 1120 (Fig. 3*C*; $P < 0.001$). Double immunofluorescence staining with Meca 32 and PDGFRβ in tumor sections from control and BIBF 1120–treated mice show a clear association of Meca 32–positive endothelial cells and PDGFRβ-positive pericytes (Fig. 3*D, top*) in the control mice, whereas in the BIBF 1120–treated mice, a marked reduction in both Meca 32–positive and PDGFRβ-positive cells was seen predominantly in the intratumoral compartment compared with the peritumoral tumor stroma separating the tumor nodules (Fig. 3*D*, area between the two dotted lines in the *right bottom*). At high magnification, a tight association between Meca 32–positive and PDGFRβ-positive cells can be seen in the tumor sample from a control mouse, but not in the BIBF 1120–treated tumor sample (Fig. 3*D, arrow* in *left top* and *bottom*). These data show not only the reduction of Meca 32–positive and PDGFRβ-positive cells upon BIBF 1120 treatment but also the loss of tight association between both cell types in the majority of the tumor vessels identified after 5 days of treatment.

***In vivo* antitumor activity associated with distinctive pharmacokinetic profile and favorable tolerability in mice.** Continuous once daily p.o. treatment of mice with established FaDu tumor xenografts at 50 or 100 mg/kg resulted in a significant inhibition of tumor growth and treated versus control (T/C) values of 27% and 11%, respectively (Fig. 4*A*). BIBF 1120 was well tolerated even in the high-dose group, with no obvious weight loss over the treatment period. Marked inhibition of tumor growth was also observed in xenograft models of human renal cell carcinoma (Fig. 4*B*; Caki-1), colorectal (HT-29), ovarian (SKOV-3), non–small

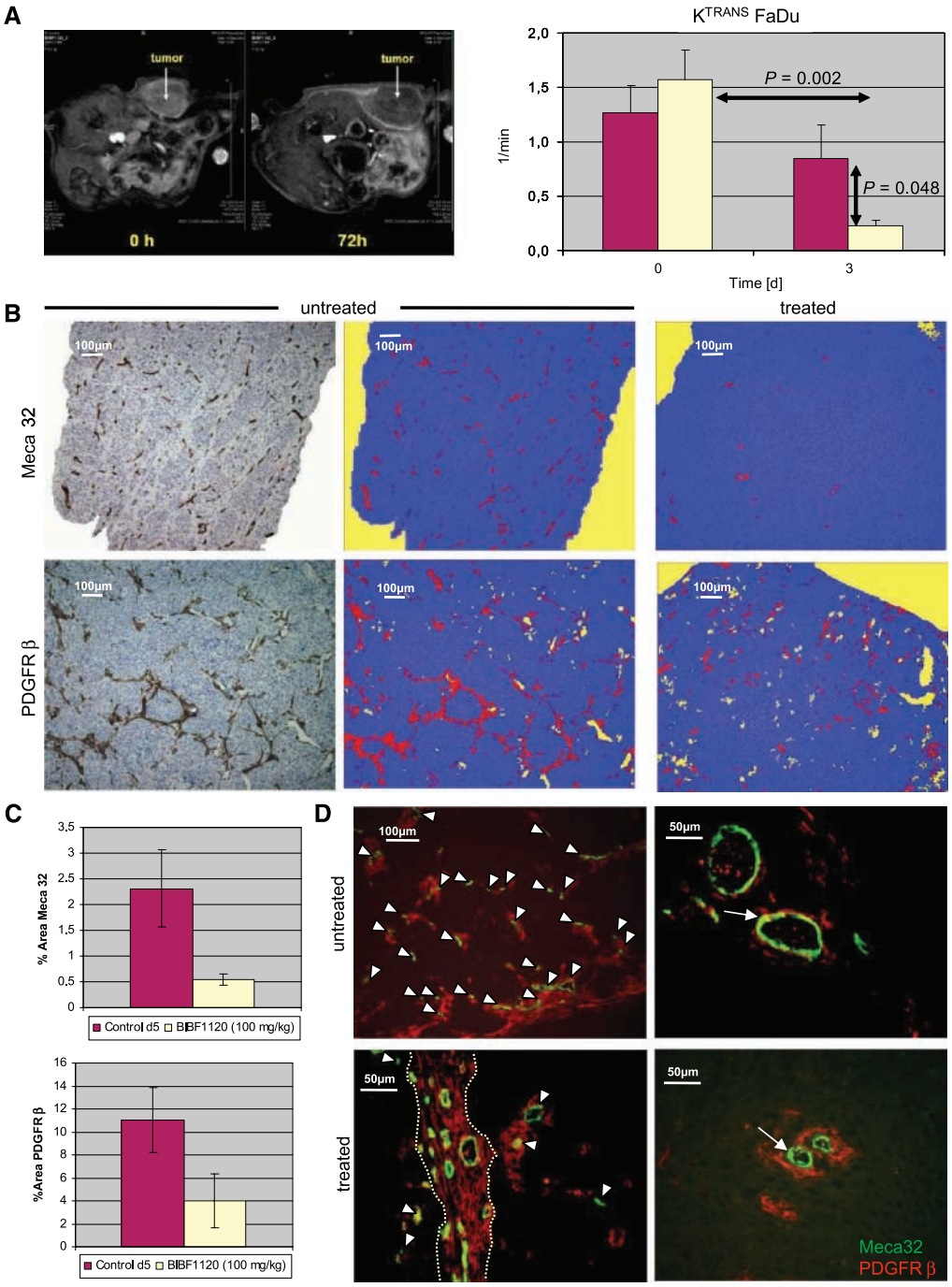

Figure 3. *A,* BIBF 1120 induces rapid changes in tumor perfusion and permeability upon treatment with BIBF 1120 in FaDu xenografts. DCE-MRI scans of tumor-bearing mice after infusion of contrast agent (Gadolinium) were taken before the treatment with BIBF 1120 and 72 h after administration of 100 mg/kg BIBF 1120. Quantification of tumor perfusion and permeability by means of Toft's model transfer constant (K^{TRANS}) after 3 d of BIBF 1120 treatment (*yellow*) compared with untreated tumors (*red*). *B,* treatment with BIBF 1120 reduces the tumor microvessel density and the number of PDGFRβ-expressing perivascular cells. Tumor sections stained with Meca 32 to detect blood vessel endothelial cells in a control mouse, the same histologic field processed for image analysis and morphometric measurement is shown in the adjacent pictures; a representative field of the image analysis processed tumor section of a BIBF 1120–treated mouse is designated as treated. *Bottom,* changes in the PDGFRβ-expressing cells in the control and treated mice. Note that some of the PDGFRβ-positive cells are associated with the tumor microvessels but others are loosely associated to the vessel wall and are located within the tumor stroma between the vessels. *Bar length,* 100 μm. *C, bar graphs*, comparison of the tumor area occupied by blood vessels covered by Meca 32–expressing endothelial cells in the control and the BIBF 1120–treated mice. Similarly, the area of the tumor containing PDGFRβ-expressing cells was determined in the control and treated mice, using the appropriate software program as described in Materials and Methods. *Columns,* means; *bars,* SD. Measurements were done in three representative histologic fields (10×) from each of the control and treated mice (n = 3 mice per group). *D,* double immunofluorescence staining for Meca 32 (*green*) and PDGFRβ (*red*) in tumor sections from control and BIBF 1120–treated mice. A reduction in both Meca 32–and PDFGRβ-expressing cells in the intratumoral compartment (*arrowheads*) of the BIBF 1120–treated mice is observed and accompanied by a loose association of endothelial cells and pericytes (*arrow in bottom right*) that contrasts with the tight association between those two cell types seen in the control mice (*arrow in top right*). The dotted lines indicate the border between tumor and peritumoral stroma tissue.

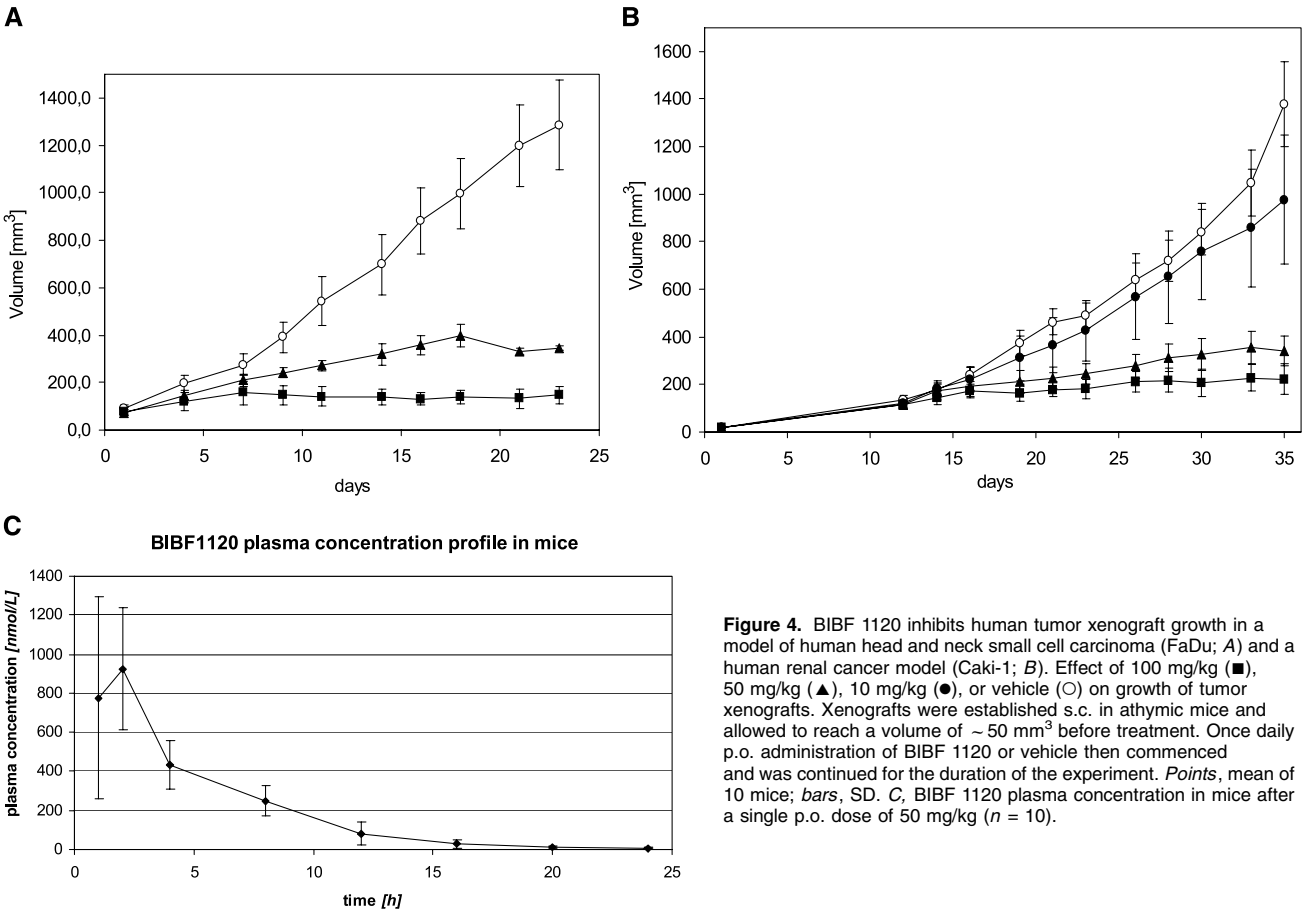

Figure 4. BIBF 1120 inhibits human tumor xenograft growth in a model of human head and neck small cell carcinoma (FaDu; *A*) and a human renal cancer model (Caki-1; *B*). Effect of 100 mg/kg (■), 50 mg/kg (▲), 10 mg/kg (●), or vehicle (○) on growth of tumor xenografts. Xenografts were established s.c. in athymic mice and allowed to reach a volume of ~50 mm^3 before treatment. Once daily p.o. administration of BIBF 1120 or vehicle then commenced and was continued for the duration of the experiment. *Points*, mean of 10 mice; *bars*, SD. *C,* BIBF 1120 plasma concentration in mice after a single p.o. dose of 50 mg/kg (n = 10).

cell lung (Calu-6), and prostate carcinoma (PAC-120), as described in Supplementary Table S1. Moreover, in a syngeneic rat glioblastoma model (cell line GS-9L), efficacy was observed at 50, 25, and 10 mg/kg with T/C values of 30%, 45%, and 74%, respectively (Supplementary Table S1). Pharmacokinetic studies after p.o. application to mice (Fig. 4*C*) revealed a maximal plasma concentration of ~1,000 nmol/L at 1 hour and trough plasma levels below 8 nmol/L at 24 hours postadministration. This distinctive pharmacokinetic profile can be explained by the rapid metabolization of BIBF 1120 by methyl ester cleavage, resulting in the generation of the main metabolite BIBF 1202 containing a free acid residue (data not shown).

Discussion

This report provides a first pharmacologic profile of the indolinone derivative BIBF 1120, an inhibitor of VEGFR, PDGFR, and FGFR tyrosine kinases with the potential to inhibit proangiogenic signaling pathways in vascular endothelial cells, as well as in pericytes and smooth muscle cells (9, 32), cell types that have attracted much recent attention as contributors to blood vessel maturation and stabilization, normal endothelial cell function, and blood flow regulation (30, 33–35).

In cell cultures, we observed that treatment with BIBF 1120 induces growth arrest and reduced survival. Our data are consistent with a key role for the VEGFR component in the mode of BIBF 1120 action. The simultaneous inhibition of FGF and PDGF signaling may open up the possibility to extend the therapeutic options for this compound in long-term cancer treatment and for other diseases as well. Indeed, in addition to the antiangiogenic and anticancer effects described in this study, we have shown in a separate series of experiments that BIBF 1120 and its close structural analogue, BIBF 1000, are highly effective in an animal model of lung fibrosis. As this pathologic condition is strongly linked to PDGF rather than VEGF signaling (36),[3] these data independently confirm that BIBF 1120 is an effective PDGF signaling inhibitor *in vivo*. Our extended biochemical profiling shows that BIBF 1120 has an attractive overall selectivity pattern in the human kinome, comparable with sorafinib, vatalanib, or cediranib (37–39). Of note, we have identified BIBF 1120 as a highly potent compound active against acute myeloid leukemia cells driven by Flt3 mutations, which may provide special benefit in this disease, beyond its antiangiogenic mode of action (29).

The pharmacologic profiling of new generation antiangiogenic compounds faces a number of technical hurdles. Most importantly, we and others have found that inhibition of the VEGF/VEGFR system alone is sufficient to fully suppress a broad range of standard human xenograft models grown s.c. in immune-deficient

[3] Unpublished observation.

mice (37–39). This contrasts sharply with the clinical observation that VEGF-targeted therapy with antibodies or small molecule kinase inhibitors is effective in a subset of cancer patients only and is commonly of limited duration (10, 40). This discrepancy suggests that, in patients, compensatory mechanisms that reinstate angiogenesis over time are triggered and standard cancer xenograft models are unlikely to reveal the molecular nature of these escape mechanisms. As a consequence, short-term xenograft models are of limited value in comparing various small molecule angiokinase inhibitors, each with a distinct profile of VEGFR, PDGFR, and FGFR inhibition, with the VEGF-specific antibody bevacizumab (41), or vatalanib (37), a prototype first-generation VEGFR kinase inhibitor. A more promising avenue to address the upside potential of new generation angiogenesis inhibitors may derive from molecularly defined animal models of cancer (42, 43) with detailed immunohistochemistry-guided studies of the architecture and functionality of tumor blood vessels. For instance, Mancuso and colleagues (34) reported that interfering with VEGF signaling alone reduces the number of endothelial cells in experimental tumors, with little effect on the associated vascular extracellular matrix and pericytes. These pericytes, in turn, served as tracks for rapid regrowth of endothelial cells upon cessation of VEGF blockade, suggesting that pericyte depletion could be an attractive added feature of antiangiogenic treatment. In our image analysis studies of BIBF 1120–treated FaDu xenografts, we observed a marked reduction of both the Meca 32–positive endothelial cells and in the compartment of PDGFRβ-labeled mural cells, consistent with a reduction in pericytes (30) and a loss of tight association between endothelial cells and pericytes. Together with our test results on isolated pericytes, it is tempting to speculate that this *in vivo* effect is mediated, at least in part, by the PDGFR inhibitory activity of BIBF 1120. In a separate line of studies, Casanovas and colleagues (20) have shown that cancer tissues are able to develop resistance against the VEGF signaling blockade by switching from VEGF secretion to alternative ligands, notably bFGF. The FGFR inhibition property of BIBF 1120 may provide the opportunity to address these types of resistance. Clearly, these investigations need to be extended and the effects of BIBF 1120 have to be explored in genetically defined cancer models, such as the RIP-Tag2 model (44), and in transgenic mouse models with simultaneous ras activation and p53 loss (42), which also have more delayed growth characteristics and more organotypic histology compared with poorly differentiated s.c. cancer xenografts.

BIBF 1120 differs from other angiogenesis inhibitors not only in its distinctive VEGFR, PDGFR, and FGFR targeting profile but also with regards to its cellular duration of action and its pharmacokinetics. Regarding its cellular mode of action, we have found a strikingly sustained inhibition of receptor activation with as yet unknown mechanistic basis. Using pulse-chase experiments with cultured cells, we could show that BIBF 1120 blocks VEGFR activation after a 1-hour exposure for >32 hours, the latest time point possible under the required cell culture conditions. Whereas BIBF 1120 is a reversible, ATP pocket-binding inhibitor, as suggested by our structural information on BIBF 1120-VEGFR cocrystals, we have not yet been able to determine specific receptor binding kinetics. However, overlapping these kinetic considerations, we have found that intracellular methylester cleavage of BIBF 1120 results in a compound, BIBF 1202, with a free acid residue and low cell membrane permeability that retained potent VEGFR-2 kinase inhibition (IC_{50}, 62 nmol/L; data not shown); its cellular trapping may contribute to the sustained mode of action. This sustained mode of cellular activity of BIBF 1120 after sufficient drug exposure may be the essential contributor to the excellent efficacy observed in tumor models and patients despite the fast *in vivo* clearance (45).[4] At the same time, there is clinical evidence that BIBF 1120 lacks some of the side effects associated with other angiogenesis inhibitors, such as hand-foot syndrome or bone marrow suppression, as well as hypertension (7, 46). One intriguing speculation is that the combination of rapid drug clearance and sustained cellular activity in highly accessible tumor vasculature may provide a window for antitumor effects combined with low propensity for hypertensive side effects, a notion that will be investigated further in the more advanced clinical testing of BIBF 1120.

Disclosure of Potential Conflicts of Interest

All authors are employees of Boehringer Ingelheim.

Acknowledgments

Received 11/19/2007; revised 4/4/2008; accepted 4/16/2008.

The costs of publication of this article were defrayed in part by the payment of page charges. This article must therefore be hereby marked *advertisement* in accordance with 18 U.S.C. Section 1734 solely to indicate this fact.

We thank Günther Adolf for critical reading of the manuscript and for scientific discussions; M. Shibuya for providing the VEGFR-2 expressing fibroblasts; and Monika Kriz, Martina Scherer, Roswitha Anglmayer, and Eva Strauss for excellent technical assistance and data evaluation.

[4] de Greef-van der Sandt ICJ, DeJongh J, Wolters JM, Schaefer HG, Roth W, Hilberg F, Danhof M, Stopfer P. Disease progression analysis of tumor growth inhibition by BIBF 1120 using population pharmacodynamic modeling. Submitted for publication. 2008.

References

1. Herbst RS. Therapeutic options to target angiogenesis in human malignancies. Expert Opin Emerg Drugs 2006; 11:635–50.
2. Morabito A, De Maio E, Di Maio M, Normanno N, Perrone F. Tyrosine kinase inhibitors of vascular endothelial growth factor receptors in clinical trials: current status and future directions. Oncologist 2006;11: 753–64.
3. Panares RL, Garcia AA. Bevacizumab in the management of solid tumors. Expert Rev Anticancer Ther 2007; 7:433–45.
4. Grandinetti CA, Goldspiel BR. Sorafenib and sunitinib: novel targeted therapies for renal cell cancer. Pharmacotherapy 2007;27:1125–44.
5. Cilley JC, Barfi K, Benson AB III, Mulcahy MF. Bevacizumab in the treatment of colorectal cancer. Expert Opin Biol Ther 2007;7:739–49.
6. Kane RC, Farrell AT, Saber H, et al. Sorafenib for the treatment of advanced renal cell carcinoma. Clin Cancer Res 2006;12:7271–78.
7. Herbst RS. Toxicities of antiangiogenic therapy in non-small-cell lung cancer. Clin Lung Cancer 2006;8 Suppl 1: S23–30.
8. Folkman J. Tumor angiogenesis: therapeutic implications. N Engl J Med 1971;285:1182–6.
9. Armulik A, Abramsson A, Betsholtz C. Endothelial/pericyte interactions. Circ Res 2005;97:512–23.
10. Jain RK. Antiangiogenic therapy for cancer: current and emerging concepts. Oncology (Huntingt) 2005;19:7–16.
11. Ferrara N. VEGF and the quest for tumour angiogenesis factors. Nat Rev Cancer 2002;2:795–803.
12. Lu D, Kussie P, Pytowski B, et al. Identification of the residues in the extracellular region of KDR important for interaction with vascular endothelial growth factor and neutralizing anti-KDR antibodies. J Biol Chem 2000; 275:14321–30.
13. Wiesmann C, Fuh G, Christinger HW, Eigenbrot C, Wells JA, de Vos AM. Crystal structure at 1.7 A resolution of VEGF in complex with domain 2 of the Flt-1 receptor. Cell 1997;91:695–704.
14. Gille H, Kowalski J, Li B, et al. Analysis of biological effects and signaling properties of Flt-1 (VEGFR-1) and KDR (VEGFR-2). A reassessment using novel receptor-specific vascular endothelial growth factor mutants. J Biol Chem 2001;276:3222–30.
15. Takahashi T, Ueno H, Shibuya M. VEGF activates protein kinase C-dependent, but Ras-independent Raf-MEK-MAP kinase pathway for DNA synthesis in primary endothelial cells. Oncogene 1999;18:2221–30.

16. Rousseau S, Houle F, Kotanides H, et al. Vascular endothelial growth factor (VEGF)-driven actin-based motility is mediated by VEGFR2 and requires concerted activation of stress-activated protein kinase 2 (stress-activated protein kinase (SAPK)2/p38) and geldanamycin-sensitive phosphorylation of focal adhesion kinase. J Biol Chem 2000;275:10661–72.
17. Carmeliet P, Lampugnani MG, Moons L, et al. Targeted deficiency or cytosolic truncation of the VE-cadherin gene in mice impairs VEGF-mediated endothelial survival and angiogenesis. Cell 1999;98:147–57.
18. Rini BI. Sorafenib. Expert Opin Pharmacother 2006;7:453–61.
19. Rini BI. Sunitinib. Expert Opin Pharmacother 2007;8:2359–69.
20. Casanovas O, Hicklin DJ, Bergers G, Hanahan D. Drug resistance by evasion of antiangiogenic targeting of VEGF signaling in late-stage pancreatic islet tumors. Cancer Cell 2005;8:299–309.
21. Cao H, Zhang H, Zheng X, Gao D. 3D QSAR studies on a series of potent and high selective inhibitors for three kinases of RTK family. J Mol Graph Model 2007;26:236–45.
22. McTigue MA, Wickersham JA, Pinko C, et al. Crystal structure of the kinase domain of human vascular endothelial growth factor receptor 2: a key enzyme in angiogenesis. Structure 1999;7:319–30.
23. Emsley P, Cowtan K. Coot: model-building tools for molecular graphics. Acta Crystallogr D Biol Crystallogr 2004;60:2126–32.
24. Legrier ME, de Pinieux G, Poirson-Bichat F, et al. [A new model of human prostate cancer, the PAC120 xenograft]. Pathol Biol (Paris) 2003;51:1–4.
25. Geyer SJ, Landay A. Immunogenetic and immunologic aspects of gliosarcoma growth in rats. Lab Invest 1983;49:436–44.
26. Steegmaier M, Hoffmann M, Baum A, et al. BI 2536, a potent and selective inhibitor of polo-like kinase 1, inhibits tumor growth *in vivo*. Curr Biol 2007;17:316–22.
27. Rupp C, Dolznig H, Puri C, et al. Mouse endosialin, a C-type lectin-like cell surface receptor: expression during embryonic development and induction in experimental cancer neoangiogenesis. Cancer Immun 2006;6:10.
28. Tofts PS, Brix G, Buckley DL, et al. Estimating kinetic parameters from dynamic contrast-enhanced T([1])-weighted MRI of a diffusable tracer: standardized quantities and symbols. J Magn Reson Imaging 1999;10:223–32.
29. Kulimova E, Oelmann E, Bisping G, et al. Growth inhibition and induction of apoptosis in acute myeloid leukemia cells by new indolinone derivatives targeting fibroblast growth factor, platelet-derived growth factor, and vascular endothelial growth factor receptors. Mol Cancer Ther 2006;5:3105–12.
30. Sennino B, Falcon BL, McCauley D, et al. Sequential loss of tumor vessel pericytes and endothelial cells after inhibition of platelet-derived growth factor B by selective aptamer AX102. Cancer Res 2007;67:7358–67.
31. Takahashi T, Shibuya M. The 230 kDa mature form of KDR/Flk-1 (VEGF receptor-2) activates the PLC-γ pathway and partially induces mitotic signals in NIH3T3 fibroblasts. Oncogene 1997;14:2079–89.
32. Bergers G, Song S. The role of pericytes in blood-vessel formation and maintenance. Neuro Oncol 2005;7:452–64.
33. Benjamin LE, Hemo I, Keshet E. A plasticity window for blood vessel remodeling is defined by pericyte coverage of the preformed endothelial network and is regulated by PDGF-B and VEGF. Development 1998;125:1591–8.
34. Mancuso MR, Davis R, Norberg SM, et al. Rapid vascular regrowth in tumors after reversal of VEGF inhibition. J Clin Invest 2006;116:2610–21.
35. Bergers G, Song S, Meyer-Morse N, Bergsland E, Hanahan D. Benefits of targeting both pericytes and endothelial cells in the tumor vasculature with kinase inhibitors. J Clin Invest 2003;111:1287–95.
36. Chaudhary NI, Roth GJ, Hilberg F, et al. Inhibition of PDGF, VEGF and FGF signalling attenuates fibrosis. Eur Respir J 2007;29:976–85.
37. Wood JM, Bold G, Buchdunger E, et al. PTK787/ZK 222584, a novel and potent inhibitor of vascular endothelial growth factor receptor tyrosine kinases, impairs vascular endothelial growth factor-induced responses and tumor growth after oral administration. Cancer Res 2000;60:2178–89.
38. Wilhelm SM, Carter C, Tang L, et al. BAY 43–9006 exhibits broad spectrum oral antitumor activity and targets the RAF/MEK/ERK pathway and receptor tyrosine kinases involved in tumor progression and angiogenesis. Cancer Res 2004;64:7099–109.
39. Wedge SR, Kendrew J, Hennequin LF, et al. CEDER-ANIB: a highly potent, orally bioavailable, vascular endothelial growth factor receptor-2 tyrosine kinase inhibitor for the treatment of cancer. Cancer Res 2005;65:4389–400.
40. Ruegg C, Mutter N. Anti-angiogenic therapies in cancer: achievements and open questions. Bull Cancer 2007;94:753–62.
41. Kim KJ, Li B, Winer J, et al. Inhibition of vascular endothelial growth factor-induced angiogenesis suppresses tumour growth *in vivo*. Nature 1993;362:841–4.
42. Shaw AT, Kirsch DG, Jacks T. Future of early detection of lung cancer: the role of mouse models. Clin Cancer Res 2005;11:4999–5003s.
43. Bergers G, Javaherian K, Lo KM, Folkman J, Hanahan D. Effects of angiogenesis inhibitors on multistage carcinogenesis in mice. Science 1999;284:808–12.
44. Hanahan D, Christofori G, Naik P, Arbeit J. Transgenic mouse models of tumour angiogenesis: the angiogenic switch, its molecular controls, and prospects for preclinical therapeutic models. Eur J Cancer 1996;32A:2386–93.
45. Mross KB, Gmehling D, Frost A, et al. A clinical, phase I pharmacokinetic (PK) and pharmacodynamic study of twice-daily BIBF 1120 in advanced cancer patients. J Clin Oncol 2005;23:3031.
46. Von Pawel J, Kaiser R, Eschbach C, et al. A double blind phase II study of BIBF 1120 in patients suffering from relapsed advanced non-small cell lung cancer (NSCLC). J Clin Oncol 2007;25:7635.